J. exp. Biol. **125**, 287–307 (1986)
Printed in Great Britain © *The Company of Biologists Limited 1986*

THE WAKE OF A JACKDAW (*CORVUS MONEDULA*) IN SLOW FLIGHT

BY G. R. SPEDDING

Department of Zoology, University of Bristol, Woodland Road, Bristol BS8 1UG

Accepted 2 June 1986

SUMMARY

The wake of a jackdaw in slow forward flight is described. The three-dimensional velocity field was investigated qualitatively and quantitatively by analysis of multiple-flash stereophotographs of the motion of neutrally buoyant helium bubbles. The best description of the wake structure appears to be a chain of planar, near-circular, discrete, small-cored, vortex loops, each produced by vorticity shed during a single downstroke.

However, the momentum measured in such a wake is approximately 35% of that required for weight support under these flight conditions. Some evidence is presented that this apparent wake momentum deficit may arise because the description of the real wake vorticity distribution is too simplistic.

The implications of these results for theoretical models of bird flight are briefly discussed.

INTRODUCTION

The work described here is a follow-on to an earlier study by Spedding, Rayner & Pennycuick (1984), in which an attempt was made to estimate the momentum and energy contained in the wake of a slow-flying pigeon by quantitative analysis of flow visualization photographs. In that case, the wake was found to consist of a series of near-circular vortex rings, much as postulated in the theoretical model of Rayner (1979*a*,*b*), but also appeared to contain only three-fifths of the momentum required to support the weight of the bird in the air. Although this calculation, and some of the measurements leading up to it, were approximate in nature, no obvious errors or dubious assumptions, either experimental or theoretical, seemed able to account for discrepancies of this magnitude. Here, the same techniques and apparatus are used to investigate the wake of a jackdaw (*Corvus monedula*) in slow flight, in order to observe whether this paradoxical result is obtained again and to find out how the differing morphology and wingbeat kinematics are reflected in the structure of the wake.

Present address: Department of Aerospace Engineering, University of Southern California, Los Angeles, CA 90089-0192, USA.

Key words: bird flight, wake, induced power.

The procedure and methodology are similar to those of the previous investigation. The wake structure will be analysed and compared with existing theoretical models (see Rayner, 1979*a*,*b*). If vortex rings are present in the wake, as one might now expect, approximate, semi-independent measures of the wake momentum and energy – and, hence, the induced power requirement – of the bird may be made. If Newton's second law is adhered to and the measured wake momentum is found to be adequate for weight support, theoretical predictions of the wake energy and induced power may be compared with the measured quantities, and the previously reported and unexplained results may be attributed to some unremarked characteristics of the pigeon flight. If, on the other hand, a large wake momentum deficit is again measured, more fundamental problems in either the experimental method and principles or the theory, or both, may be suspected.

MATERIALS AND METHODS

The bird training, experimental technique and apparatus, and photogrammetric analysis are all as documented by Spedding *et al.* (1984) and will be described only in outline here.

Experimental procedure

One jackdaw was trained to fly on a horizontal straight line along the length of a 4×2·7×1·2 m wire mesh flight cage, between two take-off platforms standing 1·5 m above the floor. After about 2 months, regular flights could be elicited by the alternate switching of two 40-W red light bulbs at either end of the cage. The experiments themselves also lasted about 2 months. In each flight down the cage, the bird passed through a cloud of approximately 2 mm diameter bubbles of helium in soap solution, which are neutrally buoyant in air. As the jackdaw passed through the bubble cloud, it would interrupt an infra-red light beam which opened the shutters of a pair of Nikon 35 mm cameras which, in turn, triggered a sequence of four Sunpak AZ5000 flashguns. In all photographs described in this paper, the delay between successive flashes was 8·0 ms, as determined by a purpose-built timer. Spedding *et al.* (1984) may be consulted for further technical details.

Immediately after completion of the bubble experiments, the jackdaw was filmed in the same flight cage at 200 frames s^{-1} by a Photosonics IPL ciné camera equipped with an Agenieux 12–120 mm lens. After filming, the bird was weighed on a Mettler electronic balance (he would stand quietly on the pan) and wing tracings of the outstretched wing were taken. The morphological and wing kinematic data are summarized in Table 1.

Photography

The resulting multiple-image stereo photographs (also referred to as stereopairs) thus record the three-dimensional flow of air around and behind the bird, down to scales where the distribution density of the bubbles or the bubble diameter becomes significant. A total of 31×2 reels of Ilford HP5 film were exposed and developed at an

Table 1. *Morphology and wingbeat kinematics of a jackdaw in slow forward flight*

Body mass	M (kg)	0·216
Wing semi-span	b (m)	0·296
Wing area	S (m^2)	0·056
Aspect ratio	A	6·01
Disc loading	N_d ($N\,m^{-2}$)*	7·80
Flight speed	V ($m\,s^{-1}$)	2·5
Stroke period	T (s)	0·18
Downstroke ratio†	τ	0·44
Stroke-plane angle	γ (degrees)	65·5
Stroke amplitude	ϕ	approx. 130
Body tilt	β (degrees)	25

* Disc loading is defined as $N_d = Mg/\pi b^2$, where g is the acceleration due to gravity.
† τ is the time spent on the downstroke divided by the stroke period, T.

equivalent speed of 800 ASA, the last five of which successfully recorded the entire wake structure for one wingbeat cycle, with full stereoscopic coverage. Enlarged lithographic positives on Ilfolith IH7 paper were made for subsequent photogrammetric analysis.

Photogrammetry

Given the camera base, B, the distance H between the cameras and the origin of some three-dimensional real space coordinate system (X, Y, Z), the focal length, f, of the lenses and (x_a, y_a), (x'_a, y'_a), the left and right photocoordinates of some point A in real space (Fig. 1), the three-dimensional coordinates (X_A, Y_A, Z_A) of that point are given by the relationships

$$X_A = B(x_a/p_a),$$

$$Y_A = B(y_a/p_a)$$

and

$$Z_A = H - B(f/p_a), \quad (1)$$

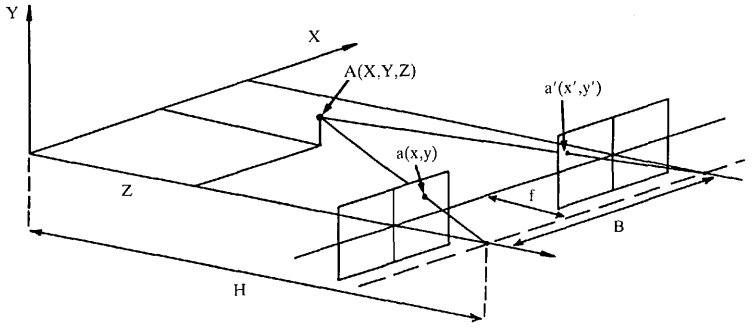

Fig. 1. The normal case geometry of a pair of stereophotographs. The parallax equations 1 may be derived by inspection of this diagram. See Materials and Methods for notation.

where $p_a = x_a - x'_a$ is the x-parallax of point A. These parallax equations are fundamental to all standard photogrammetric analyses of stereopairs; their derivation and some common applications are outlined clearly in Wolf (1974). For each point in object space (i.e. for each bubble image), x_a and x'_a were measured on a stereocomparator (a Karl Zeiss Jena Stecometer) using a floating point to locate each bubble image in stereo (i.e. in a three-dimensional perceptual space). On each stereopair, up to 2500 bubble images were digitized in this fashion, and their three-dimensional, real space coordinates were obtained by the application of equations 1.

Error analysis

Any departures from the 'normal case' geometry assumed in the parallax equations 1 (and Fig. 1) (for example, that the lens axes are parallel to each other and normal to the ground base plane XY, and the lenses are of equal and accurately specified focal length) will give rise to corresponding errors in the estimates of X, Y and Z. Errors in the determination of the position of the camera system (the elements of exterior orientation), the position of the film within the camera relative to the principal axis of the lens system (the elements of interior orientation), the position of the film in the enlarger and the orientation of the enlarger optics all affect the fidelity of the result. Possible sources of nonlinear distortion include lens aberrations, differential film emulsion shrinkage or expansion and curvature of the recording film in the camera or enlarger.

Systematic errors in the determination of X, Y and Z were compensated for by applying the collinearity condition equations to equally spaced subsets of the data field. These equations are widely used in analytical photogrammetry [see Okamoto (1981*a*,*b*) for a recent and rigorous discussion of their application in close-range photogrammetry]. On this occasion, one may exploit the fact that the camera positions are known to a reasonable degree of accuracy (±0·5 mm in H is the largest uncertainty) and that data points are evenly spread through object space with some minimum density. An ideal nonlinear correction surface is thus approximated by a composite grid of local linear corrections given by the collinearity equations. Further details are given in Spedding *et al.* (1984) which, in turn, is based entirely on the principles outlined in Hallert (1960) and Wolf (1974). Independent scalings in X, Y and Z were calculated from stereopairs of a control cube of known dimensions subjected to the same treatment. Finally, errors in the determination of bubble velocities were estimated at less than 10 %.

Calculation of velocity profiles

Generally, it proved convenient to rotate the X, Y, Z coordinate system through an angle ψ, which marked the angle between some major axis of a structure in the wake and the horizontal, so the equations

$$X' = X\cos\psi + Y\sin\psi$$

and

$$Y' = Y\cos\psi - X\sin\psi \qquad (2)$$

rotate the X, Y, Z coordinate system through an angle about Z to produce the X′, Y′, Z system where ψ is the angle between the horizontal and the new reference plane. In practice, for a wake composed of vortex rings, this amounts to a rotation of the original object space coordinates so that X′ is parallel, and Y′ perpendicular, to the plane of the vortex ring under observation. The u, v and w components of velocity in X′, Y′ and Z were then calculated for the entire data field. The coordinates and notation are sketched in Fig. 2.

All photogrammetric analysis and computation of velocity fields was performed on the Honeywell Multics system at Bristol University Computer Centre. Model calculations and ciné film analysis ran on a Research Machines 380Z microcomputer interfaced to an NAC Film Motion Analyser.

RESULTS

Vortex wake structure

Roughly 1100 stereopairs were taken, 200 of which clearly showed the complete wake structure for one wingbeat period with full stereo coverage. Simple measurements, such as wake element spacing, were taken from these 200 photographs while six stereopairs were subjected to the complete photogrammetric analysis. These were selected for some optimum, uniform bubble distribution in the wake.

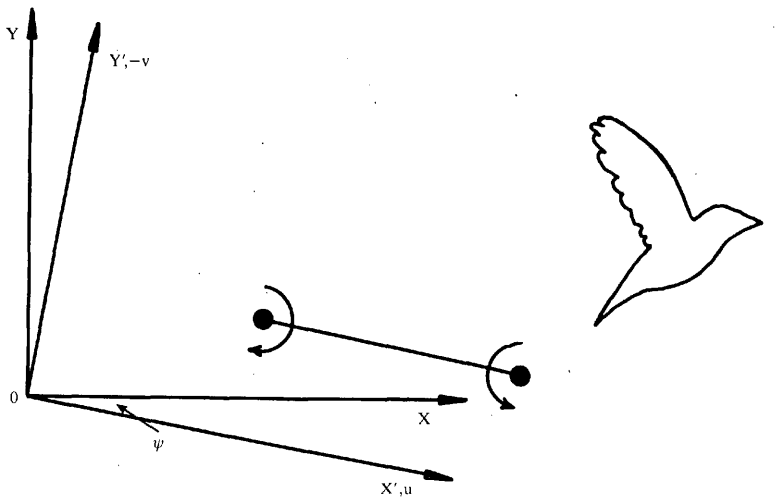

Fig. 2. Coordinate system and notation used to describe the wake. The location of the origin is determined by the left camera position in X, Y and Z(0) is set at the back wall. In a plane section, the u and v components of velocity are defined as running parallel to X′ and Y′, respectively. Note that v is defined as positive downwards.

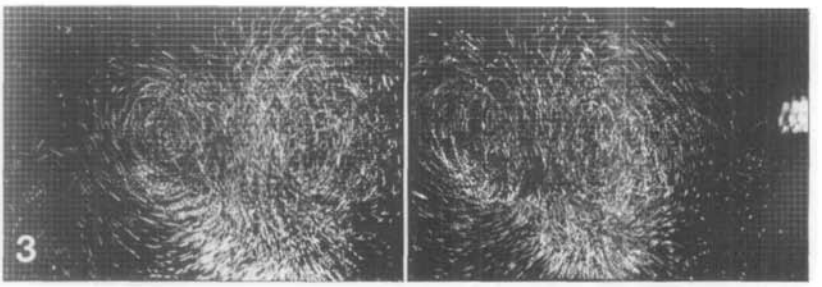

Fig. 3. Stereopair showing the wake of a jackdaw in slow flight. The bird is moving from left to right. Occasionally, bubbles appear as double streaks due to reflection of light off both front and back surfaces of the surrounding soap solution film. Time between successive flashes is 8 ms. The background grid is 2 cm square.

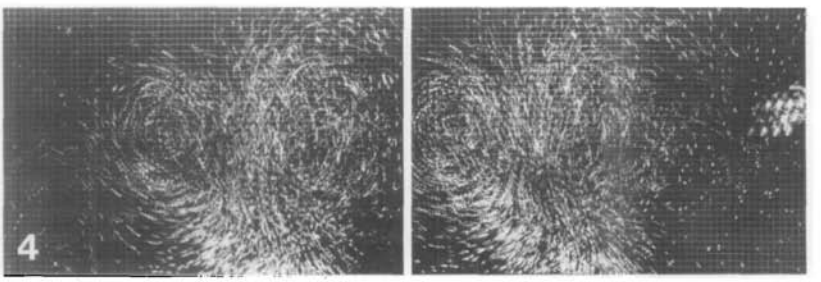

Fig. 4. Details as Fig. 3.

Figs 3 and 4 are two examples of the wake structure behind a slow-flying jackdaw where the area of stereoscopic overlap approximately covers the wake vorticity produced during one wingbeat cycle, beginning and ending at the top of the upstroke. Discrete ring-like structures can be distinguished with an induced flow winding through successive elements, which appear to be well separated. Summarizing 1100 stereopairs of qualitative information: the wake appears to be composed of discrete, planar and near-circular vortex loops and Figs 3 and 4 are examples of a pattern which is quite characteristic of these films. A closer examination and quantitative details are required before this assertion can be made with any confidence, however.

From the six stereopairs which were digitized, the data field could be reconstructed and manipulated in various ways and Fig. 5 shows the bubble field viewed

Fig. 5. Reconstructions of the bubble field: (A) from along the Z axis, and (B) plan view, from Y′. The leading bubble of each chain is denoted by a circle and the length of the trailing tail is proportional to the bubble velocity in the plane of the section.

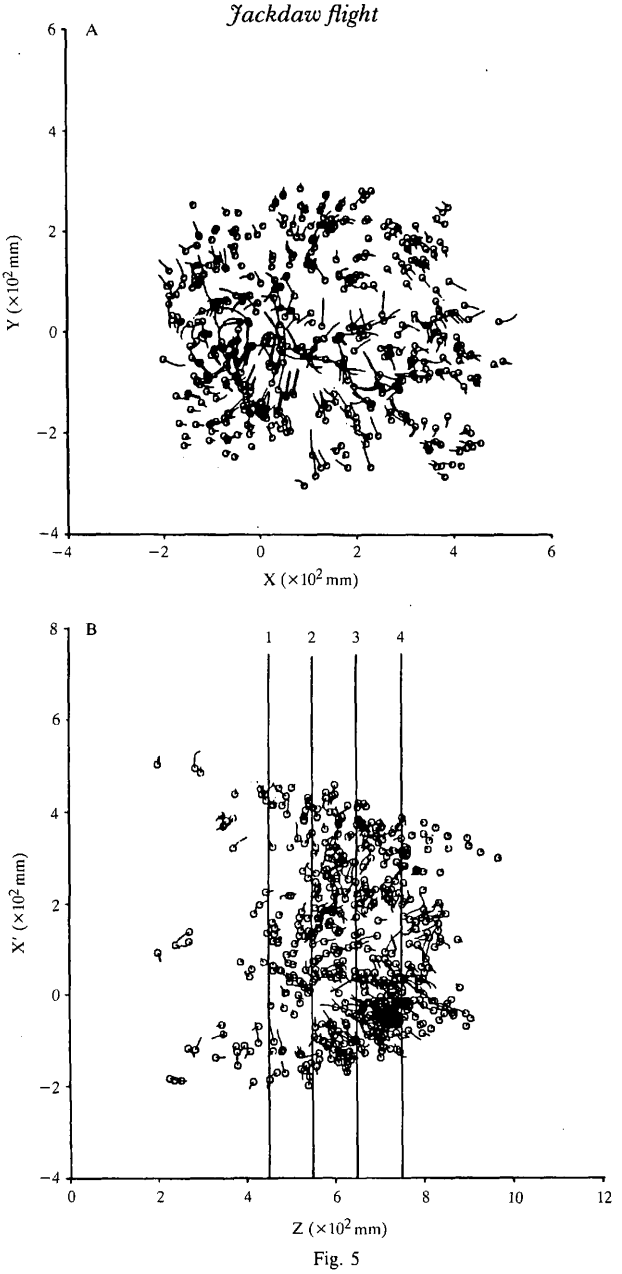
A
6
4
2
0
−2
−4
−4
−2
0
2
4
6
Y (×10² mm)
X (×10² mm)
B
8
6
4
2
0
−2
−4
0
2
4
6
8
10
12
1
2
3
4
X' (×10² mm)
Z (×10² mm)

Fig. 5

(A) from the side (along the Z axis) and (B) from above (along the Y axis). Note that the bubble coverage does not extend across the entire wake. Bubbles nearest the cameras obscure the view of those in the background and one generally has to choose which area of the wake to cover. The wake is assumed to be symmetrical about the vertical plane along the line of flight and views of bubble clouds on the far side of the wake (away from the cameras) were consistent with this assumption. The lines labelled 1–4 in Fig. 5B indicate the plane of vertical sections taken through the wake in which the velocity profiles discussed in the following section were taken.

Velocity profiles

Notation and ideal profiles

Velocity profiles were taken for a number of thin (approximately two-dimensional) sections through the three-dimensional data field, only a few of which will be described here. The purpose of these profiles is twofold: first, velocity distributions in certain sections of the wake may be compared with previously published investigations of the kinematics of vortex rings (e.g. Sallet & Widmayer, 1974; Maxworthy, 1977; Didden, 1979) to test the suitability of such a model for the wake. Second, the shape of these curves enables the calculation of several higher-order quantities in the wake for direct comparison with theoretical predictions. Note that the v component of velocity, which is perpendicular to the plane of the ring, is defined in Fig. 2 as positive downward. In this coordinate system, Fig. 6 shows three velocity profiles through an ideal vortex ring, all taken at the supposed plane of symmetry along the line of flight at Z_0. The idealized vortex ring consists of a vortex core with circular cross section which is in solid-body rotation, and an outer potential flow region where the tangential velocity is inversely proportional to the radial distance from the centre of the vortex. Such a vortex is often referred to as a Rankine vortex. Profiles A and B are the v and u velocity distributions in horizontal and vertical cuts through a vortex pair and a single circular vortex, respectively, and may be found in many classical aerodynamics texts; these are from Milne-Thompson (1966). Profile C is the distribution of v along the line of axisymmetry of a vortex ring and this curve is often integrated in experimental studies of vortex rings to estimate the total ring circulation (e.g. Didden, 1979).

Measured wake profiles

All three velocity profile are shown for four different sections through the wake in Fig. 7.1–4. Those marked A should be compared with the theoretical distributions in Fig. 6A, and so on. Thus Fig. 7.1–4A describes $v(X')$ for four Z locations across the wake at Y'_0, the plane of the ring (the centre of the vortex ring is at X'_0, Y'_0, Z_0). Sections closest to Z_0, the mid-plane, have the greatest $\partial v/\partial X'$ across the vortex core. The X′ location of the core is where $v(X') = U_s = 0{\cdot}76\,\mathrm{m\,s^{-1}}$. U_s, the mean ring convection velocity, is measured directly from bubble photographs. The velocity distribution is much as expected although there is considerable scatter (some

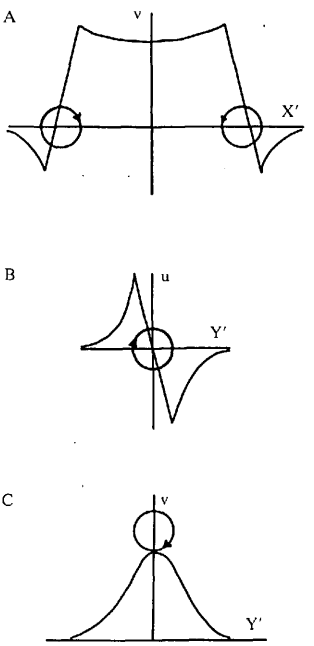

Fig. 6. Schematic velocity distributions through a Rankine vortex (B) with irrotational core and 1/r viscous decay outside and (A and C) through a vortex pair composed of two such vortices.

is to be expected because of the finite thickness of each section) and a noticeable asymmetry between the left and right core cross-sections. The scatter of points caused by section thickness is especially noticeable in sections 3 and 4, which cut obliquely across the core. The ring diameter may be estimated from the distance in X′ between left and right core cross-sections (at $v = U_s$), and having located X'_{core}, u(Y′) profiles may be taken at this point. The basic shape of the u(Y′) curve and its behaviour in sections 1–4 across the ring are both roughly as outlined in Fig. 6, but the peaks $\pm u_{max}$, which define the edge of the vortex, are less distinct. It is not clear whether this is due to the limited accuracy of the experimental technique (for example, in locating X'_{core}) or whether it indicates a more disorganized core structure. There is thus some uncertainty in the vortex core radius R_0, which is measured from the distance in Y′ between u_{max} and u_{min}. On the other hand, results from other stereopairs (Table 3) and profile A did not reveal any large inconsistencies.

The bell-shaped profile of Fig. 6C was reproduced satisfactorily near the mid-line (Fig. 7.1,2C) and velocities far from the plane of the ring tailed off quite rapidly.

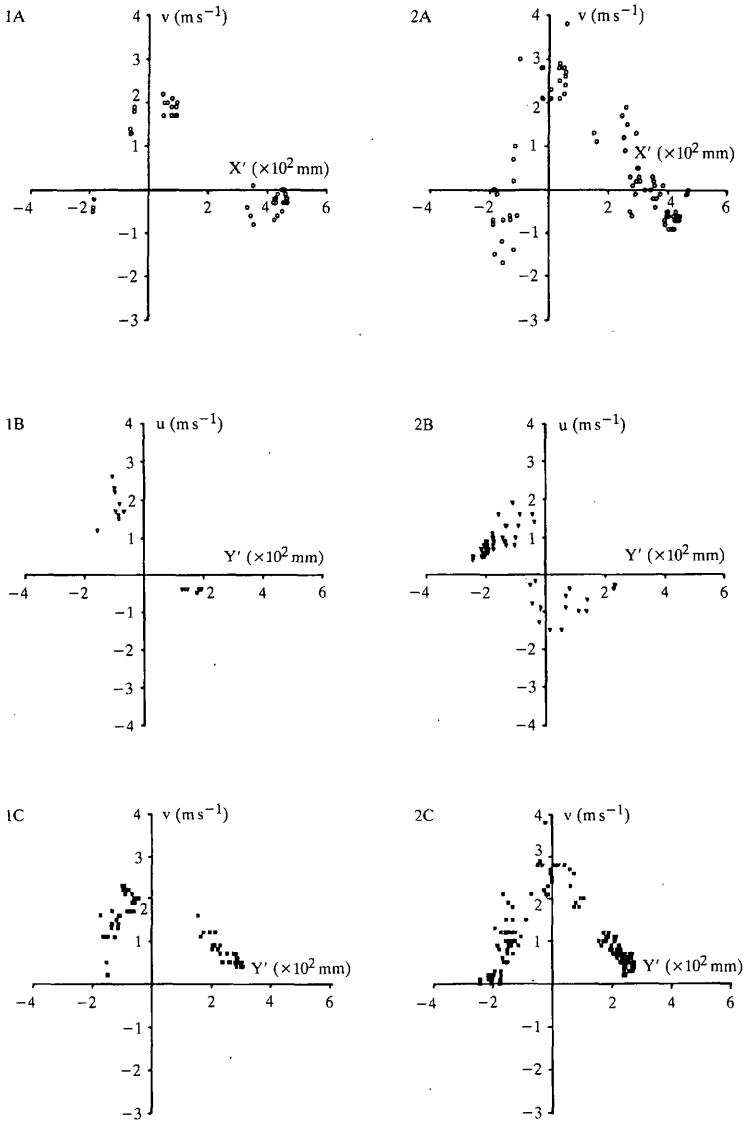

Fig. 7.1–4. Velocity profiles in sections 1–4 of Fig. 5B. Distributions labelled A–C may be compared with the ideal profiles of Fig. 6A–C. The change in shape of the profiles in sections 1–4 towards the edge of the wake is consistent with a series of sections cutting through a vortex ring. Smoothed curves of the form shown in Fig. 6 were fitted by eye through these data.

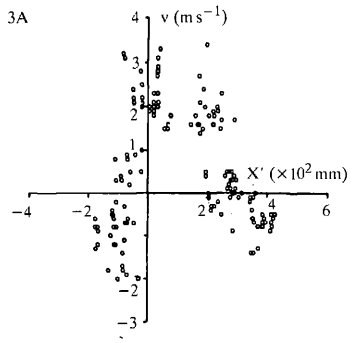
3A
v (m s^{-1})
X′ (×10^2 mm)

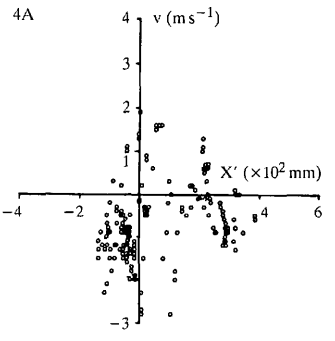
4A
v (m s^{-1})
X′ (×10^2 mm)

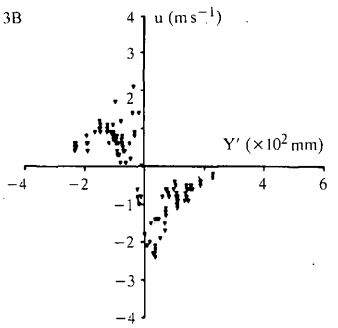
3B
u (m s^{-1})
Y′ (×10^2 mm)

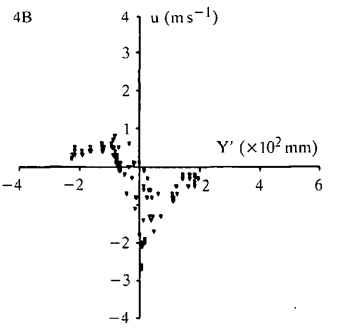
4B
u (m s^{-1})
Y′ (×10^2 mm)

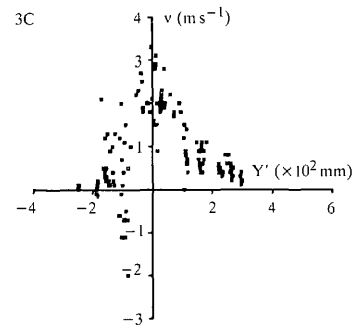
3C
v (m s^{-1})
Y′ (×10^2 mm)

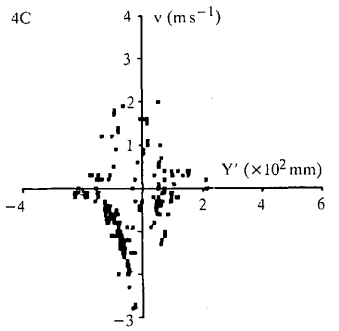
4C
v (m s^{-1})
Y′ (×10^2 mm)

This is an important result which means that one can integrate under this curve to calculate the circulation from

$$\kappa = \int_{-\infty}^{+\infty} v \, dY' \tag{3}$$

with finite data. The change in shape of $v(Y')$ from section 1 to section 4 is as expected.

Velocity profiles were mostly taken in sections parallel to the line of flight but Fig. 8 shows that the $v(Z)$ distribution is also consistent with the results thus far, up until the mid-line where the data stop, as previously noted.

The vorticity, ω, defined for a two-dimensional section in (X',Y') as

$$\omega = \partial u/\partial Y' - \partial v/\partial X', \tag{4}$$

was calculated from smoothed curves drawn through $u(Y')$ and $v(X')$ data and $\omega(r)$, where r is the radial distance from the vortex core centre, is plotted in Fig. 9. There is much uncertainty in these figures ($\pm 30\%$ would be an optimistic error estimate) and the velocity field data were not clear enough for points around R_0. Conclusions must therefore be somewhat tentative, but, while ω seems confined largely to the core of the vortex, its decline away from $r = R_0$ is more gradual than in the classical vortex ring studies (cf. Didden, 1979, figs 12, 13). It is also less well-defined than in the previously measured pigeon wake sections.

In summary, the velocity profiles behave approximately as expected for vertical sections taken through a vortex ring. Although there is some scatter in the data and some distortion of profiles A and B, the primary and only identifiable large scale structure in the wake seems to be a vortex ring. To this extent, the results of Kokshaysky (1979) and Spedding *et al.* (1984) are confirmed and the theoretical description of Rayner (1979*a*) seems appropriate.

Quantitative wake analysis

Although only six stereopairs have been analysed in full, some simple wake parameters may be measured from a larger number of single wake photographs, once the full three-dimensional analysis has shown vortex rings to be present in the wake (Table 2). The stroke period of the wingbeat was measured by ciné film analysis (Table 1) and ring convection velocities can be estimated from the spacing of successive rings in the wake. Scatter in the data here may be attributed either to the small sample size (few photographs clearly showed two rings) or to the interaction between successive rings in the wake as a newly generated ring causes its predecessor to rotate. Such behaviour was observed, and similar vortex dynamics have been demonstrated in laboratory and numerical experiments on chains of vortex rings in axially and orbitally excited jets (Lee & Reynolds, 1985; Leonard, 1985). This effect is also visible in Table 3, which presents the wake parameters estimated from the full three-dimensional analysis; the variation in ring momentum angle is much larger

than for other quantities. Although the core diameter also proved difficult to measure accurately, the mean non-dimensional core radius ($R_0/\overline{R} = 0{\cdot}141$) is still more than two standard deviations below the upper limit (0·25) where rings may be treated as small-cored (Fraenkel, 1970; Norbury, 1973).

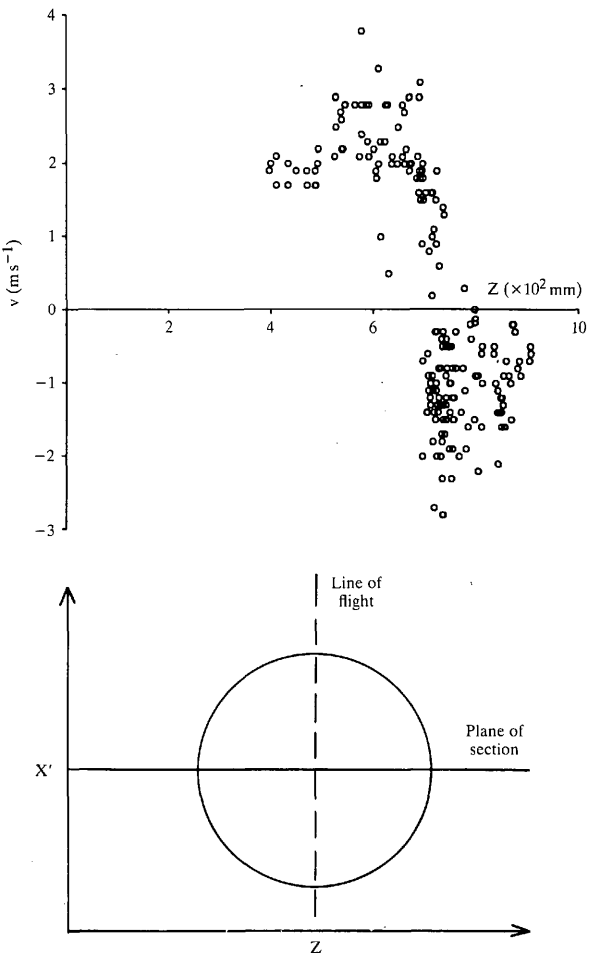

Fig. 8. v(Z) in a section perpendicular to the line of flight, across the ring centre. Symmetry about the line of flight is assumed for calculation of the ring length in Z.

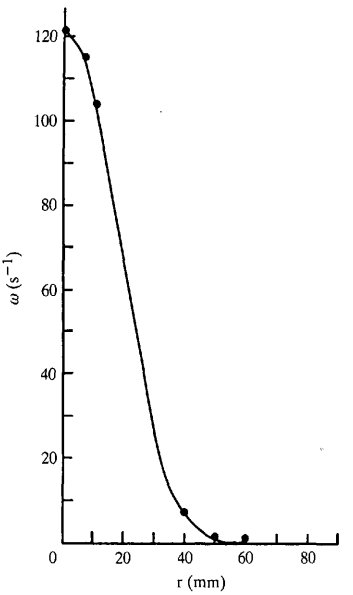

Fig. 9. $\omega(r)$. The curve through the data points has been drawn by eye. Each data point was taken from smoothed curves drawn through u(Y') and v(X') profiles at varying r.

Comparison with theory

Theoretical predictions of the wake geometry and energy and, hence, the induced power requirements were generated by an amended version of the original vortex ring model of Rayner (1979*a*), as described by Spedding *et al.* (1984). Briefly, given the wingbeat kinematics and morphological data of Table 1, and assuming an elliptical wing loading distribution, the geometry of each vortex loop in the wake may be calculated. It is stipulated that the momentum of each vortex loop must balance

Table 2. *Mean and standard deviation about the mean for quantities measured directly from single photographs*

Wake parameter	Units	Sample size (n)	Mean ($\bar{x}$)	Standard deviation (S.D.)	S.D. as % of $\bar{x}$
Apparent ring diameter	m	93	0·413	0·035	8·5
Wake element spacing:					
vertical	m	13	0·129	0·033	25·6
horizontal	m	13	0·631	0·046	7·3
Ring convection velocity	$m\,s^{-1}$	13	0·76	0·20	26·3
Ring momentum angle	degrees	93	15	3·9	26

Table 3. *Ring measurements from the complete stereophotogrammetric analysis of six jackdaw stereopairs*

	Ring length R_x (m)	Ring width R_z (m)	Core diameter R_0 (m)	$R_0/\bar{R}$*	Ring angle (ψ, degrees)	κ ($m^2 s^{-1}$)
Jackdaw 1	0·430				21·2	0·75
Jackdaw 2	0·370	0·354	0·036	0·10	10·6	0·88
Jackdaw 3	0·386	0·394	0·041	0·11	8·9	0·69
Jackdaw 4	0·390	0·384	0·068	0·17	7·0	0·72
Jackdaw 5	0·466	0·465	0·073	0·16	15·6	0·88
Jackdaw 6	0·430	0·380	0·075	0·174	10·0	0·98
$\bar{x}$	0·412	0·395	0·058	0·141	12·2	0·82
S	0·036	0·042	0·017	0·032	5·2	0·11
$S/\bar{x} \times 100$	9	11	29	23	43	14

* $\bar{R} = (R_x + R_z)/2$.

the vector sum of the parasite and profile drags of the bird, together with its weight, for the stroke period, T. The strength and orientation (κ and ψ) required for each ring to do this are calculated and the self-energy for an elliptical vortex loop of these dimensions is given by equation 43 in Rayner (1979*a*). The induced power is simply the mean rate of increase of wake kinetic energy,

$$P_i = E_s/T. \tag{5}$$

The same formula was used to calculate P_i from the experimental data but E_s was estimated from the classical equation for the energy of a circular vortex ring (e.g. Saffman, 1970),

$$E_s = 1/2\rho\kappa^2 R[\ln(8R/R_0) + \bar{A} - 2]. \tag{6}$$

The value of the constant $\bar{A}$ depends on $\omega(r)$ across the vortex core. It is not clear how the measured distribution of Fig. 9 should be expressed in terms of $\bar{A}$, so $\bar{A}$ has been assigned a value of 0·25 (as for constant ω across the core) for simplicity. Table 3 shows the eccentricity of the measured rings to be small and the true E_s should be reasonably approximated by equation 6.

The comparison between theory and experiment is detailed in Table 4. The measured ring dimensions are slightly, but consistently, smaller than predicted by the model. The ring momentum angle, ψ, is significantly greater, at least in part because of the ring interactions described earlier. The vertical wake element spacing and ring convection velocity, U_s, are both much lower than predicted. These latter discrepancies may be seen as a consequence of the significantly smaller circulations measured in the wake: $0{\cdot}82\,m\,s^{-2}$ as opposed to the predicted value of $1{\cdot}85\,m\,s^{-2}$. The difference in wake momentum is considerable, the ratio of measured momentum to that required for weight support (as enforced in the theoretical calculations) being around 0·35. In this light, the experimental estimate of the induced power requirement should be interpreted with some caution.

DISCUSSION

Interpretation of the wake analysis

The momentum deficit in the vortex wake measurements is very large. In the previous pigeon experiments this same result was attributed mainly to the small size of the rings in the wake; on this occasion the chief difference lies in the small circulation of the measured rings, and the resulting wake momentum deficit is even larger than before. The simpler wingbeat kinematics of the jackdaw have not resulted in a better agreement between experiment and theory.

Such results would be obtained if the bird was not supporting its weight but instead was losing height on the downward curve of some quasi-ballistic trajectory. Such vertical decelerations would be reflected directly in the total impulse of the wake. Two lines of evidence suggest that this is not the case. Ciné film analysis of the jackdaw flight under nearly identical conditions (continuous bright illumination and camera noise added) gave no indication of the required parabolic-shaped flight path on those occasions where the added distractions appeared not to alter the normal flight pattern. Moreover, it is possible to provide a rough estimate of the flight path during the experiments themselves by tracing multiple tail images on the bubble photographs (e.g. Figs 3, 4). From all measurable frames ($N = 66$), the mean flight path angle, a, was $-0{\cdot}23° \pm 1{\cdot}76°$. At this point, the jackdaw is usually near the end of the downstroke *following* the wingbeat which produced the measured vortex wake structure, and the small depression (and later, elevation) of the tail feathers which occurs at this stage accounts both for the small negative value of a and for the relatively large scatter around this value. In the final roll of film, the cameras were triggered earlier to show details of the flow around the wings and body, and the value

Table 4. *Wake vorticity measurements and induced power estimates as predicted by the vortex flight model and as measured by experiment*

Wake parameter	Original predictions	Measured
Ring dimensions		
Long axis (m)	0·474	0·412
Short axis (m)	0·436	0·395
Core radius (m)		0·029
$R_0/\bar{R}$	0·141*	0·141
Ring momentum angle (degrees)	0·34	12·2
Wake element spacing		
Vertical (m)	0·443	0·129
Horizontal (m)	0·437	0·631
Ring convection velocity ($m\,s^{-1}$)	2·45	0·76
Circulation ($m^2\,s^{-1}$)	1·85	0·82
Ring momentum ($kg\,m^{-1}\,s^{-1}$)†	0·362	0·126
Ring energy (J)	1·11	0·18
Induced power (W)	6·26	1·00

* Non-dimensional core radius set at measured value.
† An approximate expression for the ring momentum is $\rho\kappa\pi\bar{R}^2$, where $\bar{R}$ is the mean ring radius.

of a was $0{\cdot}22° \pm 1{\cdot}17°$ ($N = 17$). The two values of a are not significantly different from zero, or from each other, and the evidence available suggests that the jackdaw flight was indeed horizontal.

There seem to be two alternative explanations to account for the 'missing' wake momentum. The first is that some other mechanism exists for generating lift and depositing momentum into the wake. This possibility can be quickly discounted, as apart from the wings themselves the only likely candidate for such a rôle would appear to be the tail. The tail is actively depressed in synchrony with the wingbeat and a flow moving perpendicularly away from the lower tail surface can occasionally be distinguished in wake photographs. The tail area is approximately $0{\cdot}014\,m^2$ and if it accelerates an air volume of $0{\cdot}014\,m^3$ to a velocity of $3\,m\,s^{-1}$ during the course of one wingbeat ($T = 0{\cdot}18\,s$), then the rate of change of momentum of this packet of air would be $1{\cdot}205 \times 0{\cdot}014 \times 3{\cdot}0/0{\cdot}18 = 0{\cdot}28\,N$, where the air density is assumed to be $1{\cdot}205\,kg\,m^{-3}$. This is the mean force acting normal to the tail surface over one wing beat and compares with the bird's weight of $2{\cdot}06\,N$. Forces of this magnitude and orientation are more likely to be useful in stability and pitch control than to contribute significantly to weight support. They are certainly not able to account for the large wake momentum deficit, and if they were, one would still expect to detect the resulting airflow in the wake.

The remaining possibility is that the momentum exists in the wake but eludes detection. There are several ways this could occur. First, it must be admitted that the experimental procedures outlined in this and the preceding paper are based on mental or perceptual abstractions which, at least in part, duplicate the analytical abstractions of the vortex ring model which is under scrutiny. The test is not independent but guided strongly by the specific predictions of the model in question. In an ideal and thorough (and presently unrealizable) experiment the vorticity of the fluid would be measured throughout the wake, from which the impulse, **I**, is given (Batchelor, 1967) by

$$\mathbf{I} = 1/2\rho \int \mathbf{x} \times \boldsymbol{\omega}\, dV, \tag{7}$$

where $\boldsymbol{\omega}$ and $\mathbf{x}$ are the vorticity and position vectors measured in a volume element, dV. Obviously the impulse need only be measured in the fluid where $\boldsymbol{\omega}$ is non-zero. Similarly, the total kinetic energy of the fluid, T, is

$$T = \rho \int \mathbf{u}(\mathbf{x} \times \boldsymbol{\omega}) dV. \tag{8}$$

These expressions take on simpler forms when lines of vorticity organize themselves in the fluid into simple geometric shapes, for example, centring on a common axis of symmetry such as a vortex ring, when expressions like equation 6 can be derived. The analytical or experimental convenience of these simplifying assumptions is relinquished with reluctance. The argument that the wake vorticity distribution may be considerably more complex than assumed is not especially controversial but the objection might be raised that, nonetheless, no other momentum-bearing structure can be seen in the wake photographs except for the vortex rings themselves. The

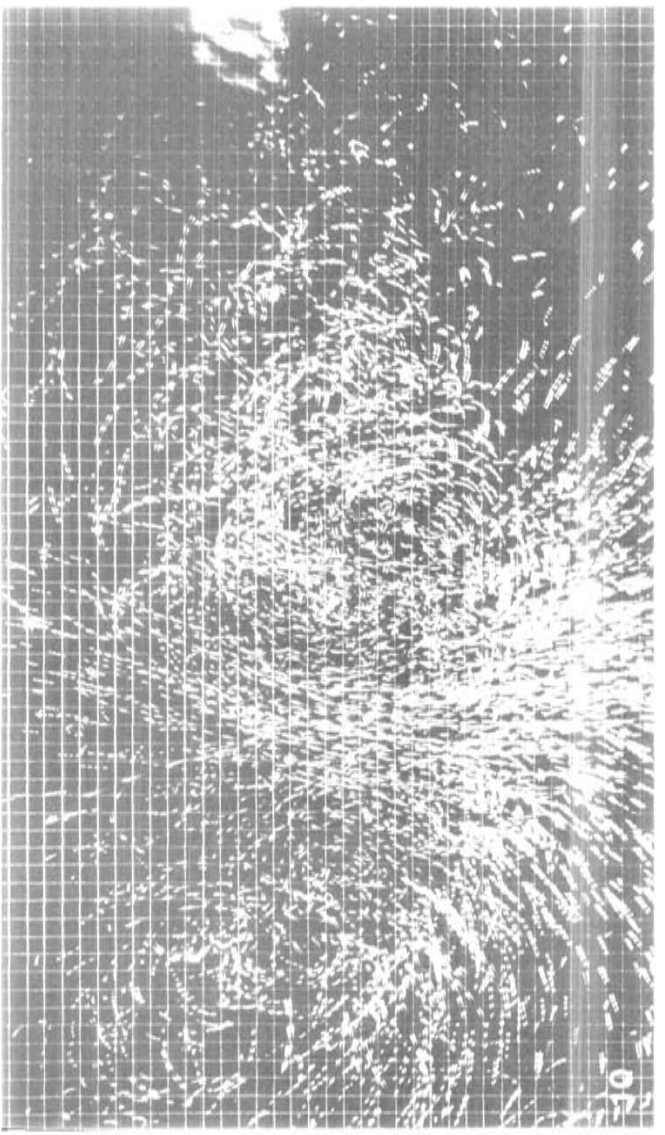

Fig. 10. Some photographs indicate that the wake vorticity distribution may be more complicated than hitherto assumed. Details as in Fig. 3.

following arguments suggest that it may be unrealistic to expect to be able to distinguish qualitatively all such wake structures, whose existence is strongly implied by the numerical results.

In a series of laboratory experiments on the dynamics of vortex rings, Maxworthy (1972, 1974, 1977) described how vortex rings moving in a real fluid deposit vorticity into a wake. The impulse contained within this wake was found to be a significant fraction of the total fluid impulse and, at ring Reynolds numbers ($Re = U_s D/v$, where D is the diameter of the generator nozzle, v the kinematic viscosity of the fluid) of 2×10^4, the circulation measured around the core of the vortex ring was about half the total circulation measured down the centreline. For comparison, the Re of the rings in the jackdaw wake is defined as $2RU/v$ and $Re = 2{\cdot}04\times10^4$. The circulation around the vortex core is

$$\kappa_{core} = 2\pi R_0 v_{core}, \tag{9}$$

where v_{core} is the tangential velocity at the edge of the core. Calculated this way, $\kappa_{core} = 0{\cdot}47\ cm\ s^{-2}$. κ_{tot}, the total circulation as measured down the centreline, is the value given in Table 4; $\kappa_{tot} = 0{\cdot}82\ cm\ s^{-2}$ and $\kappa_{core}/\kappa_{tot} = 0{\cdot}58$. This result, which is similar to that reported by Maxworthy (1977, fig. 7), indicates that there may exist a wake behind the vortex rings which accounts for a large part of the total measured impulse of the fluid, but which is not obvious from visual inspection of the photographs where the induced flow through the rings dominates the local flowfield. In this case, the wake contribution to κ_{tot} has been included by integrating velocities down the centreline of the ring, but the implication is that the wake may well contain various undetected complex structures which account for a large proportion of the total impulse (and so momentum). The results of Table 4 may in fact be interpreted as strongly supporting this hypothesis. From the data presented in Spedding *et al.* (1984) for the pigeon wake, the ratio $\kappa_{core}/\kappa_{tot}$ can be calculated as 0·61, and these arguments are equally applicable to this case.

These observations may be summarized as follows: (i) estimating the ring circulation by integrating down the ring centreline allows the vorticity in the wake of the vortex ring itself to be included in the calculation of the wake impulse; (ii) this wake behind the vortex ring accounts for a large fraction of the total measured impulse in the wake, implying that roughly half of the measured wake vorticity lies *outside* the concentrated core regions identified in the wake analysis; (iii) such a failure to measure the momentum flux in more complex distributions of wake vorticity could explain the unreasonably low estimates of wake momentum; (iv) whether or not such a 'wake' behind each vortex ring exists [the distribution of vorticity around the core of the ring could equally well be anomalous, and $\omega(r)$ (Fig. 9) was measured only at the centreline core cross-section], the real distribution of wake vorticity must be more complicated than allowed for in a simple vortex ring model; (v) such a model cannot therefore be applied to the measured wake geometry.

Some indication of the complexity of the flow field is given by a more careful inspection of Figs 3 and 4 and Fig. 10, which is a larger reproduction of one half of a stereopair whose features include an axial flow (from left to right in the

photograph, towards the bird) along the vortex core, which itself is not clearly defined on the right of the photograph. This region corresponds to the stopping vortex produced as the wings decelerate at the end of the downstroke; the roll-up of the trailing vortex sheet at this stage of the wing stroke seems to be delayed or incomplete. This observation accounts for the previously noted asymmetry of v(X') profiles across the wake.

From the numerical results, it seems that a simple vortex ring model fails as an accurate experimental description of the wake. It is concluded that vorticity shed at the wing tips and trailing edges during the wing stroke does not all roll up into a closed loop of concentrated vorticity. 'Ring' formation is clearly a complicated process and there is ample scope for energy reabsorption on the body and wing surfaces and distortion of the trailing vortex before it is identified as a distinct structure and analysed in the wake photographs. If a chain of vortex rings is the most appropriate qualitative description of the wake, it is still a simplified one which, from an experimental point of view, results in a significant amount of the wake momentum being ignored.

Applicability of the vortex ring model

In the previous section, it was argued that the vortex ring model does not adequately represent the real structure of the wake of a bird in slow horizontal flight. However, the current experiments are unable to provide a better description of the wake, nor do they indicate how it might be modelled more realistically. If the theory and experiment are both too simplistic in their approach, it does not follow that the model predictions of the induced power requirement are necessarily incorrect. Noting Lighthill's (1973) observation that vortex rings convey the maximum momentum with the minimum energy [the existence of an energy *maximum* for an axisymmetric, steadily propagating, inviscid vortex ring has been elegantly proved by Benjamin (1975)], deviations from this model pattern might be expected to increase the total wake energy for any given momentum requirement and the vortex ring model may represent some optimum minimum induced power requirement. Incidentally, there are no strong reasons why the bird should be flying with minimum energy consumption (either per unit time or per unit distance) in the experiments reported here.

Some tentative conclusions may be drawn. The vortex ring model postulated by Rayner (1979*b*) seems to be the most appropriate representation available of the wake of a slow-flying bird. As such, it may also provide the closest theoretical estimates of the power requirements in this case. As a fluid dynamical description of the wake, it also seems basically correct but does not accurately describe the complexity of the flow indicated by experiment. Consequently, experimental procedures which use the same approach may produce misleading results. On the basis of these experiments, one cannot judge the accuracy of the model predictions of the induced power requirement, P_i, nor can one assess the merits of the various alternative model calculations of P_i (e.g. Pennycuick, 1975), except to point out that the vortex ring model predictions are generally higher than the alternatives and that realistic

deviations from this pattern seem likely to increase the predicted value of P_i still further.

The author takes pleasure in thanking Dr C. J. Pennycuick for his wise counsel as academic supervisor, and for reading the first version of this manuscript. Thanks also to Dr J. M. V. Rayner who programmed all the vortex ring model computations described herein. Professors R. T. Severn and B. K. Follet (FRS) both provided invaluable support at important times and Dr K. D. Scholey was both consultant and companion throughout. Mr G. Gooding was the key interface at the University Computer Centre, Bristol. The financial support of the Science and Engineering Research Council is gratefully acknowledged.

REFERENCES

BATCHELOR, G. K. (1967). *An Introduction to Fluid Dynamics*. Cambridge: Cambridge University Press.

BENJAMIN, T. B. (1975). The alliance of practical and analytical insights into the nonlinear problems of fluid mechanics. In *Lecture Notes in Mathematics*, vol. 503, pp. 8–29. New York: Springer-Verlag.

DIDDEN, N. (1979). On the formation of vortex rings: rolling-up and production of circulation. *J. appl. Math. Phys.* **30**, 101–116.

FRAENKEL, L. E. (1970). On steady vortex rings of small cross-section in an ideal fluid. *Proc. R. Soc.* A **16**, 29–62.

HALLERT, B. (1960). *Photogrammetry*. London: McGraw-Hill.

KOKSHAYSKY, N. V. (1979). Tracing the wake of a flying bird. *Nature, Lond.* **279**, 146–148.

LEE, M. & REYNOLDS, W. C. (1985). Bifurcating and blooming jets. Report no. TF-22, Termosciences Division, Department of Mechanical Engineering, Stanford University.

LEONARD, A. (1985). Computing three-dimensional incompressible flows with vortex elements. *A. Rev. Fluid Mech.* **17**, 523–559.

LIGHTHILL, M. J. (1973). On the Weis-Fogh mechanism of lift generation. *J. Fluid Mech.* **60**, 1–17.

MAXWORTHY, T. (1972). The structure and stability of vortex rings. *J. Fluid Mech.* **51**, 15–32.

MAXWORTHY, T. (1974). Turbulent vortex rings. *J. Fluid Mech.* **64**, 227–239.

MAXWORTHY, T. (1977). Some experimental studies of vortex rings. *J. Fluid Mech.* **81**, 465–495.

MILNE-THOMPSON, L. M. (1966). *Theoretical Aerodynamics*. New York: Dover.

NORBURY, J. (1973). A family of steady vortex rings. *J. Fluid Mech.* **57**, 417–431.

OKAMOTO, A. (1981*a*). Orientation and construction of models. Part 1: The orientation problem in close-range photogrammetry. *Photogrammetric Engineering and Remote Sensing* **47**, 1437–1454.

OKAMOTO, A. (1981*b*). Orientation and construction of models. Part 4: Further considerations in close-range photogrammetry. *Photogrammetric Engineering and Remote Sensing* **48**, 1353–1363.

PENNYCUICK, C. J. (1975). Mechanics of flight. In *Avian Biology*, vol. 5 (ed. D. S. Farner, J. R. King & K. C. Parkes). London: Academic Press.

RAYNER, J. M. V. (1979*a*). A vortex theory of animal flight. II. The forward flight of birds. *J. Fluid Mech.* **91**, 731–763.

RAYNER, J. M. V. (1979*b*). A new approach to animal flight mechanics. *J. exp. Biol.* **80**, 17–54.

SAFFMAN, P. G. (1970). The velocity of viscous vortex rings. *S.I.A.M. Jl* **49**, 371–380.

SALLET, D. W. & WIDMAYER, R. S. (1974). An experimental investigation of laminar and turbulent vortex rings in air. *Z. Flugwiss.* **22**, 207–215.

SPEDDING, G. R., RAYNER, J. M. V. & PENNYCUICK, C. J. (1984). Momentum and energy in the wake of a pigeon (*Columba livia*) in slow flight. *J. exp. Biol.* **111**, 81–102.

WOLF, P. W. (1974). *Elements of Photogrammetry*. New York: McGraw-Hill.